ACS SENSORS

pubs.acs.org/acssensors Article

Microfluidic Colorimetric Biosensors Based on MnO_2 Nanozymes and Convergence–Divergence Spiral Micromixers for Rapid and Sensitive Detection of *Salmonella*

Li Xue, Nana Jin, Ruya Guo, Siyuan Wang, Wuzhen Qi, Yuanjie Liu, Yanbin Li, and Jianhan Lin*

Cite This: https://doi.org/10.1021/acssensors.1c00292 Read Online

ACCESS | Metrics & More | Article Recommendations | Supporting Information

ABSTRACT: In-field screening of foodborne pathogens plays an important role in ensuring food safety. Thus, a microfluidic biosensor was developed for rapid and sensitive detection of *Salmonella* using manganese dioxide nanoflowers (MnO_2 NFs) for amplifying the biological signal, a microfluidic chip with a convergence–divergence spiral micromixer for performing automatic operations, and a smartphone app with a saturation calculation algorithm for processing the image. First, immune magnetic nanoparticles (MNPs), the sample, and immune MnO_2 NFs were fully mixed and sufficiently incubated in the spiral micromixer to form MNP–bacteria–MnO_2 sandwich complexes, which were magnetically captured in a separation chamber in the microfluidic chip. Then, a 3,3′,5,5′-tetramethylbenzidine (TMB) substrate was injected and catalyzed by a MnO_2 NF nanomimetic enzyme on the complexes, resulting in the production of yellow catalysate. Finally, the catalysate was transferred into a detection chamber and its image was measured and processed using the smartphone app to determine the number of bacteria. This biosensor was able to detect *Salmonella* from 4.4×10^1 to 4.4×10^6 CFU/mL in 45 min with a detection limit of 44 CFU/mL, and has the potential to provide a promising platform for on-site detection of foodborne bacteria.

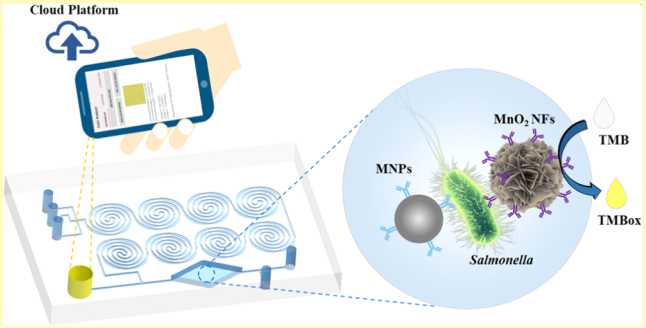

KEYWORDS: *colorimetric biosensor, microfluidic chip, convergence–divergence spiral micromixer, MnO_2 nanoflowers, smartphone app*

Foodborne pathogens have resulted in numerous illnesses annually and caused huge economic losses globally.[1] According to the World Health Organization (WHO), *Salmonella* is one of the major global causes for diarrheal diseases and one of the microorganisms with emerging resistant serotypes.[2] The Centers for Disease Control (CDC) estimated that *Salmonella* led to 1.35 million infections with 26 500 hospitalizations and 420 deaths in the US every year.[3] The key to prevent and control Salmonellosis is effective and rapid detection of *Salmonella* in the food supply chains from farm to fork.[4]

To date, detection of *Salmonella* in a food sample basically relies on culture plating, which is considered as the gold standard in many countries and international organizations. However, the culture method requires a long time up to 2 days to obtain the final result. As a result, it is unsuitable for rapid detection of foodborne *Salmonella*. Enzyme-linked immunosorbent assay (ELISA) has been recommended as a rapid method for *Salmonella* detection, but it is often able to detect *Salmonella* as low as only 10^3 CFU/mL due to low efficiency for a solid–liquid reaction, which cannot meet the demand for food safety. In addition, conventional ELISA methods are generally susceptible to false positives due to cross contaminations.[5] Therefore, it is urgently needed to develop new methods for rapid and sensitive detection of *Salmonella*. As alternatives, various types of biosensors, including optical,[6] electrochemical,[7] and piezoelectric,[8] have been attempted for rapid detection of foodborne pathogens. As an important branch of optical biosensors, a colorimetric biosensor has shown its merits of contactless detection, low cost, and easy integration, and thus has become a powerful analytical tool for bacterial detection.

In recent years, various nanomimetic enzymes, as a new generation of artificial enzymes, have attracted considerable attention and made great progress due to their unique properties of effective catalysis, easy synthesis, good stability, and low cost.[9] So far, many nanomimetic enzymes, such as manganese dioxide nanoflowers/nanosheets,[10] gold nanoparticles,[11] platinum nanoparticles,[12,13] palladium nanoparticles,[14] and metal–organic frameworks (MOFs),[15] have been

Received: February 11, 2021
Accepted: June 29, 2021

Scheme 1. Schematic of this Colorimetric Biosensor for Detection of *Salmonella*

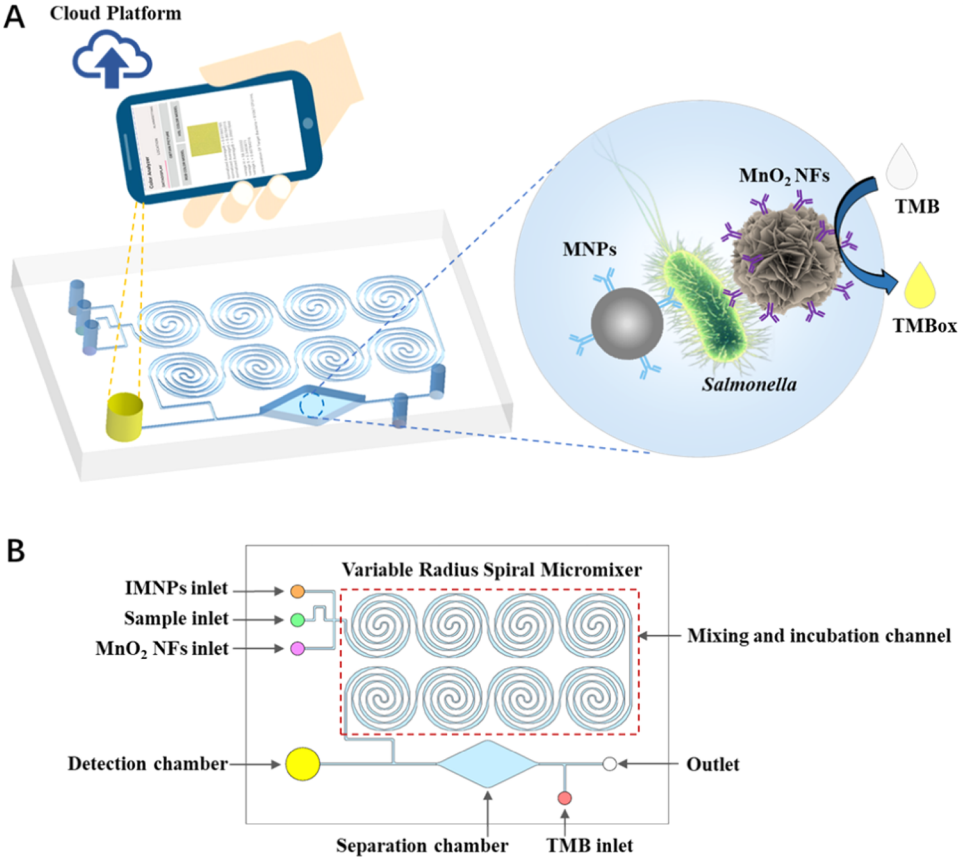

successfully developed and used for the development of biosensors. In particular, much attention has been paid to manganese dioxide nanoflowers (MnO_2 NFs) since they are featured with outstanding physical and chemical properties, including a high surface area, tunable size, good biocompatibility, and stable peroxidase-mimic characteristics.[16] In addition, a microfluidic chip, known as lab-on-a-chip, has also come into increasing focus because it owns the tremendous ability to integrate mixing, reaction, separation, and detection onto one chip and has the obvious advantage of automatic fluidic operation, less reagent consumption, and rapid reaction.[17−19] A micromixer plays an important role in the design of microfluidic chips because a very low Reynolds number indicates that the fluids are in a laminar flow regime, which has a great impact on reaction. Thus, some new micromixers have been developed using various geometric structures to improve the mixing efficiency.[20,21] Recently, some interesting studies were reported about convergent−divergent micromixers, which were demonstrated with excellent mixing performance.[22−24] Therefore, the combination of a MnO_2 nanoflower mimic nanoenzyme and a convergence−divergence micromixer might provide a new platform for rapid detection of pathogens.

In the past decade, smartphones have been frequently used with ELISA to develop portable colorimetric biosensors due to their great merits, including widespread popularity, low cost, user-friendly interface, in-built wireless communication, and strong image analysis ability.[25,26] A typical example was reported by Zeinhom et al. using the magnetic nanoparticles and the horseradish peroxidase (HRP) antibody-inorganic nanoflower-based ELISA, and a smartphone microplate reader for rapid detection of *Salmonella enteritidis* in dairy food and water samples. This biosensor was demonstrated with the ability to detect *S. enteritidis* as low as 1 CFU/mL in 3 h.[27] In our previous studies, we have also developed some optical biosensors combing immunomagnetic separation, smartphone image analysis, and/or a microfluidic chip.[28,29] Although these biosensors have achieved rapid detection of foodborne bacteria, tedious magnetic separation and washing procedures were still performed manually.

To simplify the operation, shorten the time, and reduce the cost, this study intended to develop a lab-on-a-chip biosensor for rapid and sensitive detection of *Salmonella* using MnO_2 NFs for amplifying the biological signal and a microfluidic chip with a convergence−divergence spiral micromixer for performing the automatic operations. As shown in Scheme 1, immune magnetic nanoparticles (MNPs), the sample, and immune MnO_2 NFs were first injected into the microfluidic chip simultaneously, and completely mixed by the new convergence−divergence spiral micromixer to form the MNP−bacteria−MnO_2 sandwich complexes, which were magnetically captured in a separation chamber. Then, a 3,3′,5,5′-tetramethylbenzidine (TMB) solution was injected and catalyzed by the MnO_2 NFs on the complexes, and the catalysis reaction was terminated with hydrochloric acid (HCl). Finally, the catalysate was analyzed in a detection chamber using a smartphone image App to determine the concentration of *Salmonella*, and the result was combined with the sampling information and transmitted to a cloud platform via WiFi for real-time risk assessment. The novelty of this study mainly included the following points: (1) the MnO_2 NFs with higher mimic enzymatic activity and better stability were used

https://doi.org/10.1021/acssensors.1c00292
ACS Sens. XXXX, XXX, XXX−XXX

as signal probes for effective amplification of the biological signals; (2) the microfluidic chip with the convergence−divergence spiral micromixer was developed to achieve sufficient immunoreaction, effective magnetic separation, and efficient enzymatic catalysis on the chip and thus greatly enhance the consistence; and (3) the smartphone app with a built-in saturation calculation algorithm was developed for accurate measurement of the color change, and the detection results can be combined with the sampling location (GPS) and time, which can be directly obtained from the smartphone, and transmitted to the food safety monitoring cloud platform through wireless communication for real-time risk assessment.

MATERIALS AND METHODS

Materials. Streptavidin-modified MNPs (150 nm, 1 mg/mL) from Ocean Nanotech (San Diego, CA, https://www.oceannanotech.com) were used with the anti-*Salmonella* cAbs (2.85 mg/mL) from Meridian (Memphis, TN, https://meridianlifescience.com) for magnetic separation of the target *Salmonella* cells. Hydrochloric acid (HCl) and poly(vinylpyrrolidone) (PVP) from Sigma-Aldrich (St. Louis, MO, https://www.sigmaaldrich.com) and potassium permanganate ($KMnO_4$) from Sinopharm Chemical (Beijing, China, https://www.sinoreagent.com) were used for synthesis of the MnO_2 NFs. 3-Aminopropyl triethoxysilane (APTES) from Aladdin (Shanghai, China, https://www.aladdin-e.com) was used to modify the amino groups onto the MnO_2 NFs. The anti-*Salmonella* dAbs (2.5 mg/mL) from Abcam (Cambridge, MA, https://www.abcam.com) were used with the MnO_2 NFs for specifically labeling the *Salmonella* cells. TCO-PEG4-NHS ester (TCO) and tetrazine-sulfo-NHS ester (Tz) from Click Chemistry Tools Bioconjugate Technology (Scottsdale, AZ, https://clickchemistrytools.com) were used for modifying the detection antibodies onto the surface of MnO_2 NFs. 3,3′,5,5′-Tetramethylbenzidine (TMB) and phosphate-buffered saline (PBS, 10 mM, pH 7.4) from Solarbio (Beijing, China, http://www.solarbio.com) were used as a catalytic substrate and a buffer solution, respectively. Bovine serum albumin (BSA, 1%, w/v) from EM Science (Gibbstown, NJ, http://www.emscience.com) was prepared in PBS for blocking. Tween-20 from Amresco (Solon, OH, http://www.amresco-inc.com) was prepared in deionized water for washing. Deionized water produced by Advantage A10 from Millipore (18.2 MΩ·cm, Billerica, MA, http://www.merckmillipore.com) was used for preparing all of the solutions. The silicone elastomer kit from Dow Corning (Sylgard 184, Auburn, MI, https://consumer.dow.com/en-us.html) was used for fabricating the microfluidic chip. The Objet30 Pro 3D printer and the printing material from Stratasys (Eden Prairie, MN, https://www.stratasys.com) were used for fabricating the mold of the microfluidic chip.

Design and Fabrication of the Microfluidic Chip. The microfluidic chip was developed using three-dimensional (3D) printing. As shown in Scheme 1B and Figure S1, the microfluidic chip (60 mm long × 40 mm wide × 6 mm high) consists of three components: (1) a micromixer with eight convergence−divergence spirals for effectively mixing the MNPs, a sample, and MnO_2 NFs and sufficiently incubating the mixture to form the MNP−bacteria−NF sandwich complexes, (2) a rhombohedron separation chamber with the length of 15 mm, the width of 7 mm, and the height of 2 mm for magnetically separating the complexes from the sample background by applying an external magnetic field below the separation chamber, and (3) a detection chamber to house the catalysate for image collection and analysis using a self-developed smartphone app.

For fabrication of the microfluidic chip, the mold of the microchannel was first designed using SolidWorks software (Concord, MA) and printed using the Objet30 Pro 3D printer. Then, the mold was cast with the poly(dimethylsiloxane) (PDMS) prepolymer and the curing agent at the mass ratio of 10:1 and cured at 65 °C for 12 h. Finally, the PDMS replica was peeled off from the mold and bonded onto a glass slide to form the microfluidic chip after surface plasmon treatment.

Development of the Smartphone App. An android smartphone (Type, Huawei, Shenzhen, China) was employed to collect the image using its built-in high-resolution camera and analyze the image using a self-developed app. As shown in Figure S2, this app includes three functions: (1) image snap and analysis, (2) sampling location and display, and (3) risk assessment and warning. After the image of the catalysate in the detection chamber was collected by commanding the image capture program to use the built-in camera, the peripheral area of the collected image was cropped to reduce the background noise and only the central area (3 mm × 3 mm) was used for further analysis. The red−green−blue (RGB) value of each pixel in the central area was obtained and converted into the hue−saturation−lightness (HSL) color space through the matrix transformation algorithm, and the average saturation value was calculated to determine the amount of *Salmonella* based on the calibration model between the saturation of the image and the concentration of the target bacteria. In addition, the GPS information (longitude and latitude) of the sampling location was automatically obtained using the android application programing interface (API) and real-time displayed on the built-in electronic map. The detection result was combined with the GPS information and wirelessly sent to a food safety monitoring cloud platform via WiFi for risk assessment and early warning.

Culture and Enumeration of the Bacterial Cultures. *Salmonella typhimurium* was used as target bacteria. *Escherichia coli* O157:H7, *Listeria monocytogenes*, *Staphylococcus aureus*, *Bacillus cereus*, and *Vibrio parahaemolyticus* were used as the nontarget bacteria. All of these bacterial strains were stored at −20 °C in a glycerol/broth medium (30%, v/v) and reactivated by incubating the bacteria in a sterile Luria−Bertani (LB) medium (Aoboxing Biotech, Beijing, China) at 37 °C for 16−24 h with shaking at 180 rpm. The bacterial cultures were 10-fold diluted with sterile PBS to obtain the bacteria at the concentrations of 10^1−10^6 CFU/mL. Bacterial enumeration was conducted using the standard culture plating. In brief, the bacterial samples were serially 10-fold diluted with sterile PBS, and 100 μL of the diluents were surface plated on the LB agar plates. After incubation at 37 °C for 22−24 h, the visible colonies were counted for enumeration of the bacteria.

Preparation of the MNPs and MnO_2 NFs. The immune magnetic nanoparticles were prepared by conjugating the biotinylated capture antibodies with the streptavidin-modified MNPs according to the binding of biotin and streptavidin. In brief, 20 μg of the streptavidin-modified MNPs was first mixed with 4 μg of the biotinylated capture antibodies and incubated for 45 min at 15 rpm, then washed with PBST (PBS containing 0.05% Tween-20) to remove the surplus antibodies, and finally suspended in 500 μL of PBS (pH 7.4, containing 1% BSA) and stored at 4 °C for further use.

The immune MnO_2 nanoflowers were prepared based on our previous report with slight modifications.[30] For the synthesis of the MnO_2 nanoflowers, after 100 mL of $KMnO_4$ (0.1 M) was mixed with 10 mL of PVP (26 mg/mL) under stirring and heated to 80 °C, 100 mL of HCl (0.2 M) was added and incubated for 1 h. Then, the mixture was cooled to room temperature and centrifuged at 12 000 rpm for 10 min to remove the supernatant. Finally, the pure MnO_2 NFs were obtained after washing with deionized water three times. For the modification of the MnO_2 NFs, the synthesized MnO_2 NFs were first functionalized with amino groups through APTES. Then, the MnO_2 NFs and detection antibodies were functionalized with TCO and Tz, respectively. Finally, the TCO-functionalized MnO_2 NFs and the Tz-functionalized dAbs were mixed at 15 rpm for 30 min to obtain the immune MnO_2 NFs through a reaction between Tz and TCO.

Establishment of the Calibration Model. Prior to the test, the detection chamber was sealed by tape, and 1% BSA was used to block the channel for 30 min to minimize the nonspecific adsorption. The same volume (200 μL) of the immune MNPs (20 μg), *S. typhimurium* with different concentrations from 4.4×10^1 to 4.4×10^6 CFU/mL, and the immune MnO_2 NFs (40 μg) were first injected, respectively, at a flow rate of 10 μL/min using the precise syringe pumps (Pump 11 elite, Harvard Apparatus, Holliston, MA). After they were fully

https://doi.org/10.1021/acssensors.1c00292
ACS Sens. XXXX, XXX, XXX−XXX

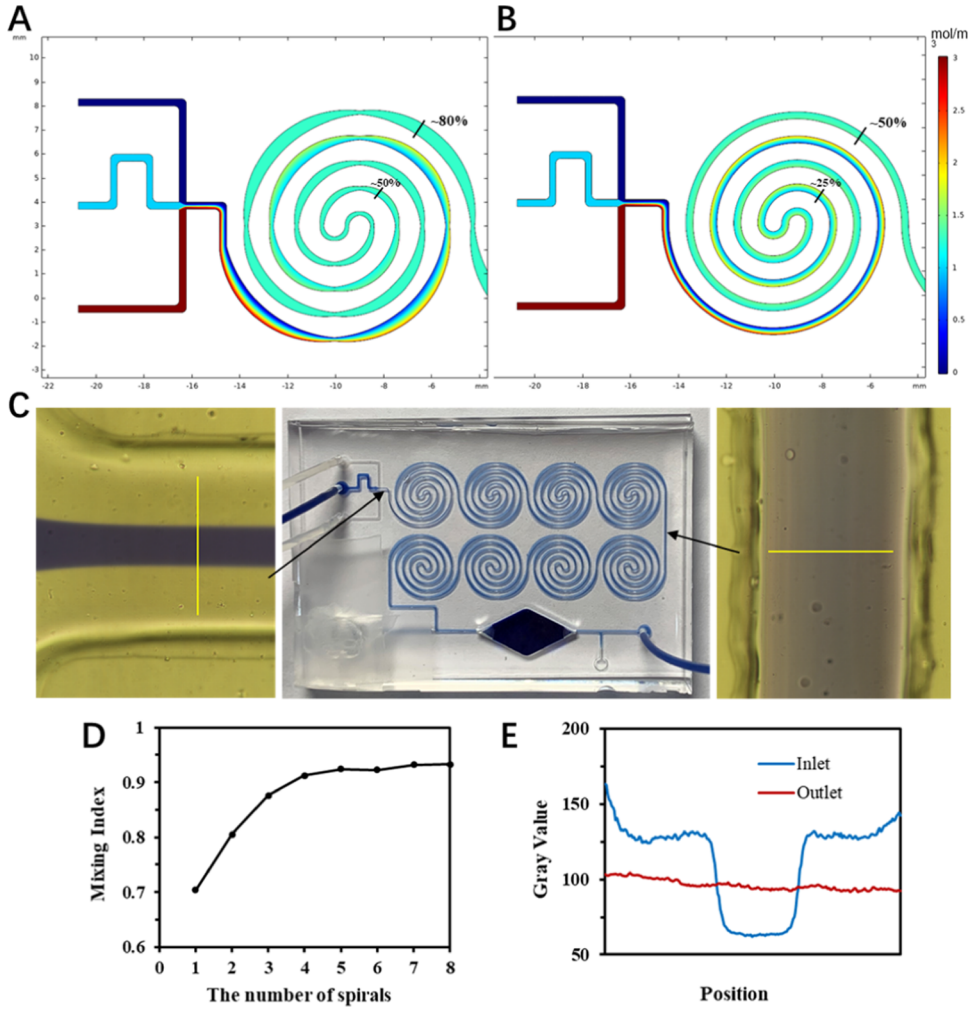

Figure 1. Mixing effect of this convergence−divergence spiral micromixer (A) and the traditional spiral micromixer (B), (C) experimental result for the convergence−divergence spiral micromixer of the microfluidic chip, (D) mixing efficiency for different numbers of convergence−divergence spirals, and (E) gray value analysis on the images of the inlet and the outlet.

mixed and incubated in the convergence−divergence spiral micromixer, the sandwich complexes were formed and captured in the separation chamber by applying an external magnet below the chamber, followed by washing with 500 μL of PBST at a flow rate of 100 μL/min to remove the unbound immune MnO_2 NFs. Then, 100 μL of TMB was injected into the chamber, catalyzed for 5 min, and terminated with 50 μL of HCl (1 M). Finally, the catalysate was transferred to the detection chamber, and its image was collected and analyzed using the smartphone app to obtain the saturation value, which was linearly related with the logarithm of the bacterial concentration to establish the calibration model of this biosensor.

Detection of the Target Bacteria in Spiked Chicken Samples. The applicability of this colorimetric biosensor was evaluated using this biosensor to detect *Salmonella* in spiked chicken samples. The chicken meat was purchased from a local supermarket and verified to be free of *Salmonella* using selective culture plating. According to China's food safety national standards for detection of bacteria in foods (GB 4789), 25 g of each chicken meat was first added into 225 mL of sterile PBS and homogenized using a stomacher (BagMixer, InterScience, Paris, France) for 4 min, followed by standing for 15 min to obtain the supernatant. Then, different concentrations of the pure *Salmonella* cultures were added into the supernatant to prepare the spiked samples with the bacterial concentrations from 5.6×10^1 to 5.6×10^4 CFU/mL. Finally, three parallel tests on each spiked sample with the volume of 200 μL were conducted using both the biosensor and the standard culture plating. The recovery was calculated as the ratio of the readout of this biosensor to that of culture plating.

RESULTS AND DISCUSSION

Mixing Efficiency of the Micromixer. The mixing efficiency of a convergence−divergence spiral micromixer in the microfluidic chip has a great impact on the sensitivity of this biosensor. It was simulated using finite element analysis software COMSOL (5.4a, Burlington, MA). As shown in Figure 1, the mixing efficiency of the convergence−divergence spiral micromixer (~80%) is obviously higher than that of the traditional spiral one (~50%). This is because the convergence−divergence structure of this micromixer enhances the mixing effect. The simulated mixing efficiency (M_e) at the cross section of the mixing channel is defined as follows

$$M_e = 1 - \frac{\sqrt{\frac{1}{n}\sum_{i=1}^{n}(c_i - c_m)^2}}{c_m} \quad (1)$$

where, c_i is the concentration of the point i, c_m is the average concentration of all of the points, and n is the total number of the points at the cross section.

To verify the actual mixing effect of this micromixer, the blue dye (medium) and the deionized water (top and bottom)

https://doi.org/10.1021/acssensors.1c00292
ACS Sens. XXXX, XXX, XXX−XXX

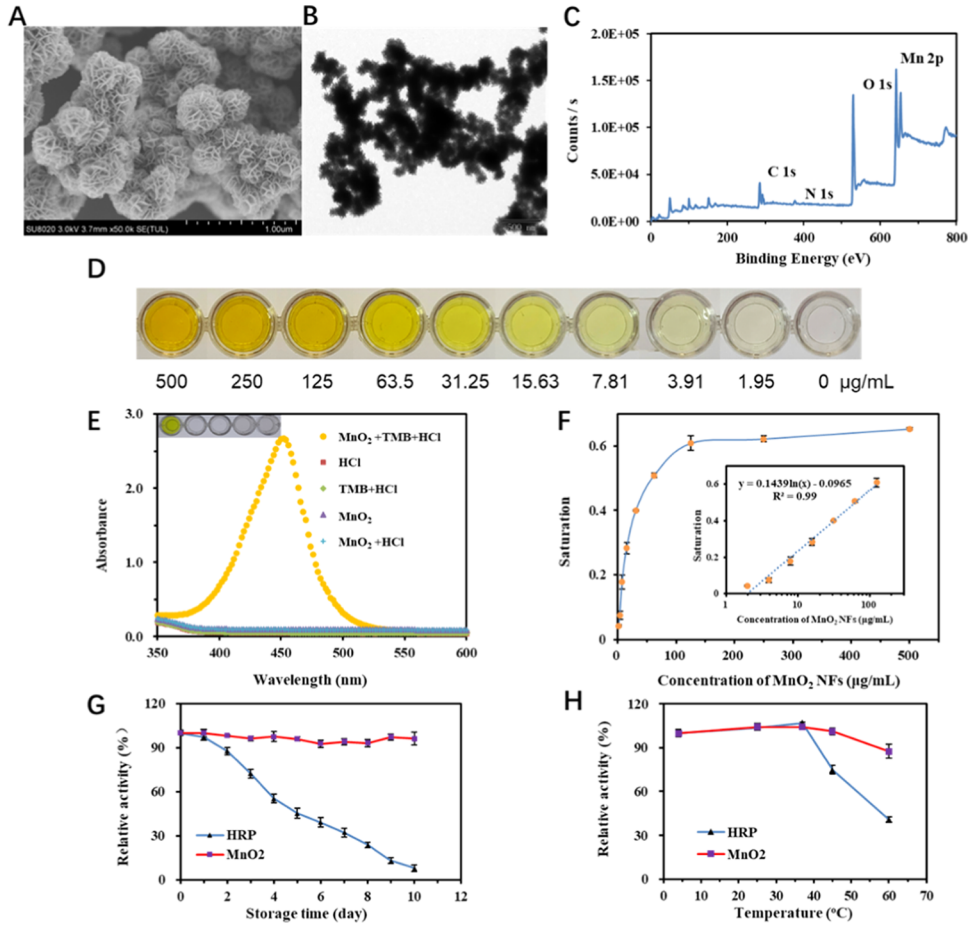

Figure 2. SEM image (A), TEM image (B), and XPS spectrum (C) of the MnO_2 NFs; (D) color changes for different concentrations of immune MnO_2 NFs to catalyze the TMB substrate; (E) absorption spectra for MnO_2 + TMB + HCl, HCl, TMB + HCl, and MnO_2 and MnO_2 + HCl; (F) relationship between the saturation value and the concentration of MnO_2 NFs, the inset shows the calibration curve between the saturation value and the concentration of MnO_2 NFs ranging from 1.95 to 125 μg/mL (N = 3); (G) comparison of enzymatic activity of the MnO_2 NFs and HRP at different storage times (N = 3); and (H) comparison of the enzymatic activity of the MnO_2 NFs and HRP at different temperatures (N = 3).

were simultaneously injected into the micromixer at the same flow rate (100 μL/min), and the images at the inlet and the outlet were collected using a microscope (Ti-E, Nikon, Tokyo, Japan, www.microscope.healthcare.nikon.com) (see Figure 1C). The mixing index (MI) of the micromixer is characterized by calculating the concentration variance of the mixture at the cross section and can be expressed as follows

$$\sigma = \sqrt{\frac{1}{N-1}\sum_{i=1}^{N}(X_i - \bar{X}_i)^2} \quad (2)$$

$$\mathrm{MI} = 1 - \sqrt{\frac{\sigma^2}{\sigma_{\max}^2}} \quad (3)$$

where σ is the standard deviation, X_i is the normalized color intensity of pixel i, $\bar{X}_i$ is the average normalized color intensity of all of the pixels, MI is the mixing index, and $\sigma_{\max}$ is the maximum standard deviation at the inlet. The images were processed using the image processing software (ImageJ) to obtain the color intensity of the pixels. As shown in Figure 1D, the mixing efficiency of this micromixer reaches 90% when three fluids flow through four convergence–divergence spirals at a flow rate of 100 μL/min. Because the immunoreaction between the target bacteria and the capture/detection antibodies takes certain time,[31] additional four convergence–divergence spirals were established for incubation to allow a sufficient reaction. To further understand the mixing effect, the gray values of the images at the inlet and the outlet were analyzed by ImageJ software. As shown in Figure 1C,E, two clear boundary lines appear at the inlet and the gray values from top to bottom have three obvious levels, indicating that these three solutions are clearly separate. In addition, the color looks uniform at the outlet and the gray values are basically consistent, indicating these solutions are well mixed. Thus, this convergence–divergence spiral micromixer was demonstrated with an excellent mixing effect.

The reasons for using this diverging–converging spiral micromixer include: (1) Although the traditional spiral micromixer can achieve the same mixing efficiency by increasing the number of the units/length, only adding the units/length of the conventional spiral micromixer will inevitably increase the size of the mixer and thus result in increasing cost. Thus, the diverging–converging structure was used to improve the mixing effect, and Figure 1 shows that the mixing efficiency of the convergence–divergence spiral micromixer (~80%) is obviously higher than that of the traditional spiral one (~50%) with the same length. (2) The immunoreaction between the target bacteria and the capture/detection antibodies takes certain time, and our previous study has verified that the dynamic incubation could greatly enhance the

https://doi.org/10.1021/acssensors.1c00292
ACS Sens. XXXX, XXX, XXX−XXX

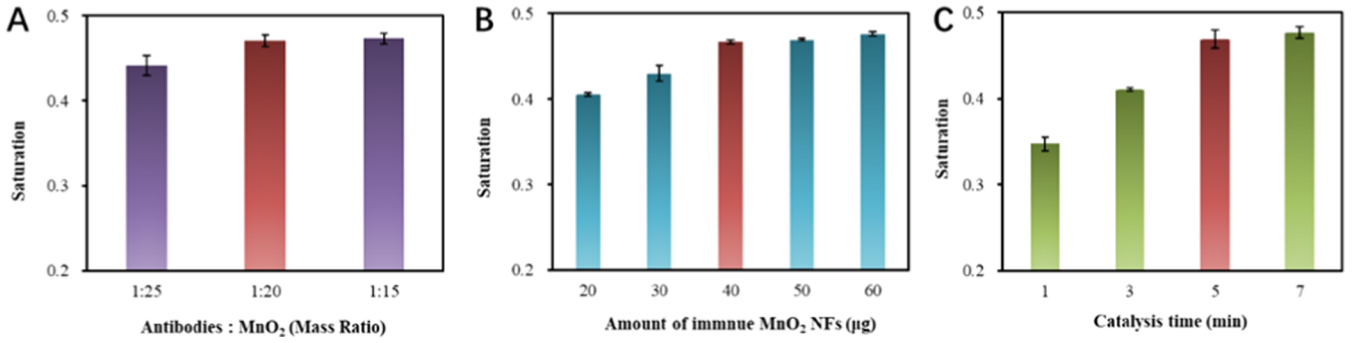

Figure 3. Optimization of the biosensor: (A) amount of antibodies, (B) amount of immune MnO_2 NFs, and (C) catalysis time.

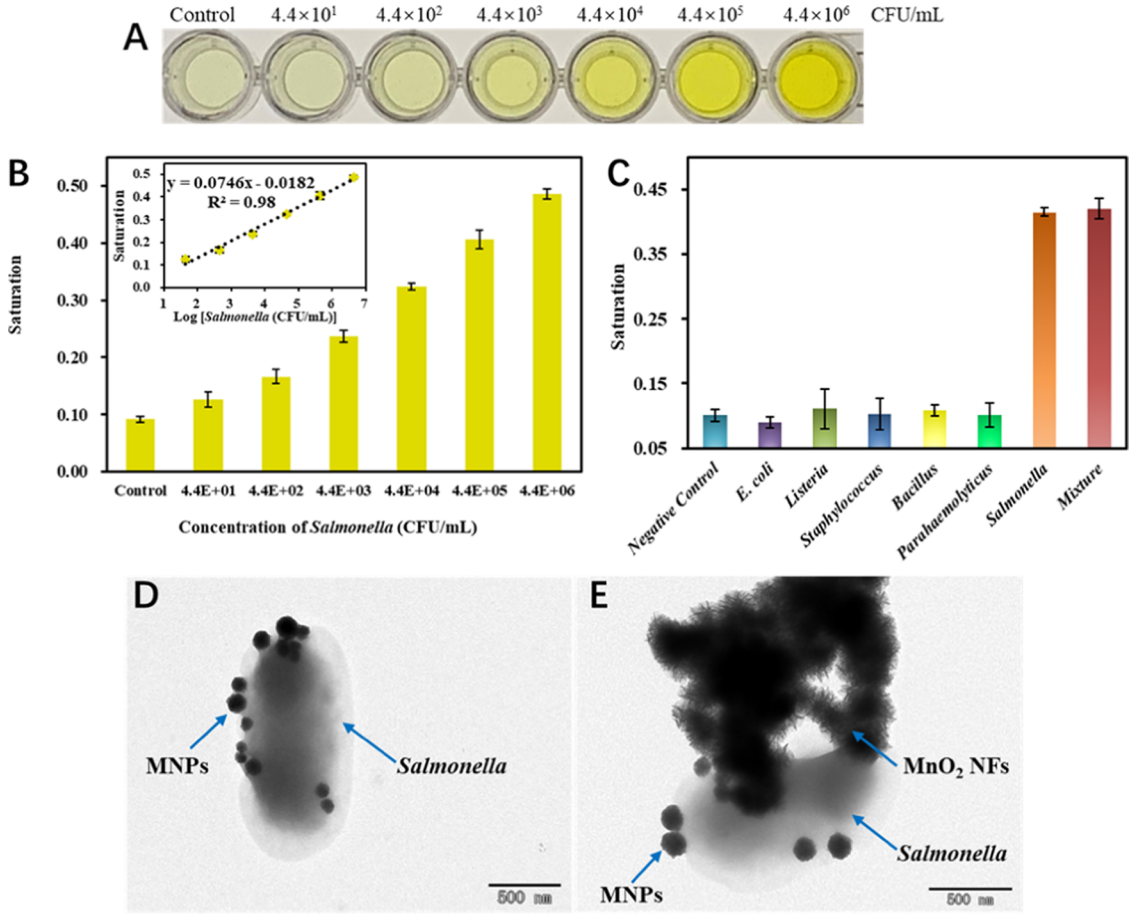

Figure 4. (A) Visible color change of the catalysate for different concentrations of *S. typhimurium*. (B) Calibration curve of this biosensor for detection of *Salmonella* ranging from 4.4×10^1 to 4.4×10^6 CFU/mL ($N = 3$). (C) Specificity of this biosensor to the nontarget bacteria ($N = 3$); the TEM images of the MNP-*Salmonella* (D) and MNP-*Salmonella*-MnO_2 (E) complexes.

efficiency of the immune reaction.[32] Thus, four convergence−divergence spiral structures were added for incubation to allow the sufficient reaction. (3) The mold of the micromixer was fabricated using 3D printing, which could accurately print very complex structures in short time and at low cost.

Characterization of the MnO_2 NFs. The MnO_2 NFs were used as nanomimetic enzymes to improve the sensitivity in this study and played an important role in this biosensor. Thus, the scanning electron microscopy (SEM), transmission electron microscopy (TEM), and X-ray photoelectron spectroscopy (XPS) spectrum were used to characterize the MnO_2 NFs. As shown in Figure 2A,B, the SEM and TEM images show that the MnO_2 NFs have a uniform flower-like structure with a lot of flakes and their average size is ∼200 nm. As shown in Figures 2C and S3, the XPS spectrum displays the C 1s (284.8, 292.1, 295.1 eV), N 1s (399.5 eV), O 1s (530.1 eV), and Mn 2p (Mn $2p_{3/2}$: 642.1 eV, Mn $2p_{1/2}$: 654.1 eV) peaks, confirming the successful synthesis of the MnO_2 nanoflowers.[33] In addition, the peroxidase-like characteristic of the MnO_2 NFs was verified using 2.5 μg of MnO_2 NFs (in 50 μL of deionized (DI) water) to mix with/without a TMB substrate, incubating for 5 min, and terminating with HCl. Their absorption spectra between 350 to 600 nm were recorded. As shown in Figure 2E, only when the MnO_2 NF mixes with TMB and HCl, the color is obviously yellow, while the others are almost colorless. These results show that the

https://doi.org/10.1021/acssensors.1c00292
ACS Sens. XXXX, XXX, XXX−XXX

Table 1. Comparison of This Biosensor with Other Reported Methods for Bacteria Detection

methods	instrument	LOD (CFU/mL)	linear range (CFU/mL)	total time (h)	refs
photothermal	thermal sensor	300	3.0×10^2–1.0×10^3	1.5	35
PCR[a]	PCR amplifier	10^3	10^3–10^7	2	36
fluorescent	fluorescence spectrometer	300	2.0×10^3–4.5×10^7	1	37
electrochemical	electrochemical workstation	50	10^2–10^7	1	7
colorimetric	color distance-based detection	100	10^2–10^4	1.5	38
colorimetric	UV–vis spectrometer	22	1.0×10^2–1.0×10^5	0.62	39
colorimetric	smartphone	10	4×10^5– 4×10^8	12	40
colorimetric	smartphone	44	4.4×10^1–4.4×10^6	0.75	this study

[a]PCR: polymerase chain reaction.

MnO_2 NFs have good peroxidase-like enzymatic activity. Furthermore, different concentrations (1.95–500 μg/mL) of the MnO_2 NFs were used to catalyze the TMB substrate and the saturation value was measured using a smartphone app. As shown in Figure 2D,F, the saturation value increases with the concentration of the MnO_2 NFs and the saturation value (S) has a good linear relationship with the concentration (C) of MnO_2 NFs ranging from 1.95 to 125 μg/mL, indicating the feasibility of the MnO_2 NFs as label.

Since the bioactivity of this nanoenzyme is crucial to this biosensor, the bioactivity of MnO_2 NFs under different conditions was investigated and compared to horseradish peroxidase (HRP). Figure 2G shows that the MnO_2 NFs retain more than 92% of their original mimic enzymatic activity after they were stored at room temperature for 10 days; however, HRP lost almost 90% of its original enzymatic activity under the same conditions. This indicates that the MnO_2 NFs have excellent storage stability. For in-field applications, temperature is usually not controllable. Thus, the MnO_2 NFs and HRP at different temperatures from 4 to 60 °C were investigated. As shown in Figure 2H, the enzymatic activity of HRP decreases with increasing temperature, and more than 60% of the biological activity is lost when the temperature reaches 60 °C. However, the MnO_2 NFs retain more than 87% of their original mimic enzymatic activity under the same conditions, indicating they have much better temperature tolerance than HRP.

Optimization of the Biosensor. The amount of detection antibodies for conjugation with MnO_2 NFs, the amount of immune MnO_2 NFs, and the catalysis time have a great impact on the sensitivity of this biosensor. To obtain the optimal amount of detection antibodies, 600 μg of the MnO_2 NFs was mixed with the detection antibodies at different antibodies-to-MnO_2 NFs mass ratios of 1:25, 1:20, and 1:15 to prepare the immune MnO_2 NFs for detection of *Salmonella* at 3.2×10^6 CFU/mL. Figure 3A shows that the saturation value for the mass ratio of 1:20 is lower than that for 1:25 and similar with that for 1:15, indicating that 30 μg of the antibodies is sufficient for conjugation with the MnO_2 NFs. Thus, the optimal antibodies-to-MnO_2 NFs mass ratio was 1:20. In addition, different amounts of immune MnO_2 NFs were used for detection of *Salmonella* at 1.0×10^6 CFU/mL. Figure 3B shows that the saturation value increases from 0.40 to 0.46 when the amount of immune MnO_2 NFs changes from 20 to 40 μg. However, a further increase to 60 μg only results in a 1% increase in the saturation value, indicating that 40 μg is sufficient for labeling the target bacteria with the concentrations of 10^6 CFU/mL or less. Therefore, the optimal amount of 40 μg for the immune MnO_2 NFs was used in this study. In addition, different catalysis time (1, 3, 5, and 7 min) were used for the optimal amount of MnO_2 NFs to catalyze the TMB substrate. Figure 3C shows that the saturation value changes from 0.35 to 0.47 when the catalysis time increases from 1 to 5 min, and remains at the same level after 7 min, meaning that 5 min is sufficient for MnO_2 NFs to catalyze the TMB substrate. Thus, the optimal catalysis time was 5 min.

Sensitivity and Specificity of the Biosensor. Under the optimal conditions, the calibration model between the saturation value and the concentration of target bacteria for this biosensor was established to determine the concentration of *Salmonella* in an unknown sample. Three parallel tests on pure culture *Salmonella* cells with different concentrations of 4.4×10^1–4.4×10^6 CFU/mL were detected using this biosensor. Figure 4A shows that the bacteria samples with higher concentrations have greater color changes. As shown in Figure 4B, a good linear relationship between the saturation value (S) and the logarithm of the bacterial concentration (C) is found and can be expressed as $S = 0.0746*\log(C)-0.0182$ ($R^2 = 0.98$). The limit of detection for this biosensor was determined to be 44 CFU/mL based on three times signal-to-noise ratio,[34] which was 2–3 orders of magnitude lower than that for the HRP-based conventional ELISA method (3.4×10^4 CFU/mL, see Figure S4). To further confirm the formation of the sandwich complexes, TEM imaging was used to characterize the MNP–bacteria complexes and the MNP–bacteria–MnO_2 NFs complexes. The images shown in Figure 4D,E, verify their successful formation.

Compared with some recently reported methods for bacterial detection, this colorimetric biosensor showed higher sensitivity, shorter time, and/or greater portability (see Table 1). This is mainly attributed to the following aspects: (1) the MnO_2 NFs with higher mimic enzymatic activity and better stability were used as signal probes for effective amplification of biological signals; (2) the microfluidic chip with a convergence–divergence spiral micromixer was developed to achieve sufficient immunoreaction, effective magnetic separation, and efficient enzymatic catalysis on the chip and thus greatly enhance the consistence; (3) the smartphone app with a built-in saturation calculation algorithm was developed for accurate measurement of the color change. The whole bacterial detection procedure was completed within 45 min.

The specificity of this biosensor was evaluated by detecting the target bacteria (*Salmonella*), the nontarget bacteria (*E. coli*, *Listeria*, *Staphylococcus*, *Bacillus*, and *Parahaemolyticus*), and their mixture at a concentration of 10^6 CFU/mL. As shown in Figure 4C, it is obvious that the saturation values of the nontarget bacteria (0.090 for *E. coli*, 0.111 for *Listeria*, 0.103 for *Staphylococcus*, 0.109 for *Bacillus*, and 0.101 for *Parahaemolyticus*) are much lower than those of *Salmonella* (0.415)

https://doi.org/10.1021/acssensors.1c00292
ACS Sens. XXXX, XXX, XXX–XXX

and their mixture (0.420), verifying that this biosensor has good specificity.

Applicability of the Colorimetric Biosensor. The practical applicability of this biosensor was evaluated by detecting the target bacteria in spiked chicken meat samples. Three parallel tests on spiked chicken meats were conducted using this biosensor. The results were compared with the gold standard culture plating and are shown in Table 2. The

Table 2. Detection of *Salmonella* in Spiked Chicken Samples Using This Biosensor

culture (CFU/mL)	detected (CFU/mL)	recovery (%)	RSD (%)
56	73	130.36	8.55
560	516	92.14	8.26
5600	5036	89.93	7.41
56 000	49 207	87.87	6.76

recoveries for chicken samples at concentrations of 5.6×10^1 to 5.6×10^4 CFU/mL were 130.4, 92.1, 89.9, and 87.9%, respectively, and the mean relative standard deviation of these samples was less than 8.6%. There was no significant difference between the readouts from this biosensor and those from the standard culture-plating method, indicating that this biosensor had good applicability for detection of *Salmonella* in chicken meat samples.

The combination of the MnO_2 NF mimic enzyme, the smartphone app, and the microfluidic chip with the convergence−divergence spiral micromixer are well-articulated to develop the portable, easy-to-use, and low-cost biosensor for rapid, sensitive, and in-field detection of foodborne pathogens. The app on the universal and cheap smartphone was first considered to replace the traditional benchtop instrument and tested to verify its capability for quantitative measurement of the color. Then, the MnO_2 NFs with higher mimic enzymatic activity was introduced to replace a traditional biological enzyme (such as HRP) for labeling the target bacteria to produce a more obvious color change, and the parameters were optimized to match the linear detection range of the smartphone app. Finally, the microfluidic chip was developed to automatically perform the bacterial detection procedure to reduce the human error and skill requirement, and the convergence−divergence spiral structure was designed to further shorten the immune reaction time.

CONCLUSIONS

In this study, we have successfully developed a colorimetric biosensor using a microfluidic chip with a convergence−divergence spiral structure and the MnO_2 NFs nanomimetic enzyme for rapid and sensitive detection of *Salmonella*. This biosensor was able to detect *Salmonella* from 4.4×10^1 to 4.4×10^6 CFU/mL in 45 min with a detection limit of 44 CFU/mL. The MnO_2 NFs were verified with a good peroxidase-like enzymatic activity and excellent environment tolerance, thus enhancing the sensitivity of this biosensor. The convergence−divergence spiral micromixer was demonstrated with great mixing efficiency. In addition, the smartphone app was confirmed to be a perfect platform for in-field image processing and wireless data transmission. This biosensor has been evaluated with high sensitivity, good specificity, and feasible applicability for detection of *Salmonella* and may provide a promising platform for on-site detection of foodborne pathogens.

ASSOCIATED CONTENT

Supporting Information

The Supporting Information is available free of charge at https://pubs.acs.org/doi/10.1021/acssensors.1c00292.

Photo of the microfluidic chip, the interfaces of the smartphone app, XPS spectra of the MnO_2 NFs, and experimental results for detection of *Salmonella* ranging from 3.4×10^1 to 3.4×10^6 CFU/mL using the HRP-based ELISA method (PDF)

AUTHOR INFORMATION

Corresponding Author

Jianhan Lin − *Key Laboratory of Modern Precision Agriculture System Integration Research, Ministry of Education, China Agricultural University, Beijing 100083, China;* orcid.org/0000-0001-9458-1077; Email: jianhan@cau.edu.cn

Authors

Li Xue − *Key Laboratory of Agricultural Information Acquisition Technology, Ministry of Agriculture and Rural Affairs, China Agricultural University, Beijing 100083, China*

Nana Jin − *Key Laboratory of Agricultural Information Acquisition Technology, Ministry of Agriculture and Rural Affairs, China Agricultural University, Beijing 100083, China*

Ruya Guo − *Key Laboratory of Agricultural Information Acquisition Technology, Ministry of Agriculture and Rural Affairs, China Agricultural University, Beijing 100083, China*

Siyuan Wang − *Key Laboratory of Agricultural Information Acquisition Technology, Ministry of Agriculture and Rural Affairs, China Agricultural University, Beijing 100083, China*

Wuzhen Qi − *Key Laboratory of Agricultural Information Acquisition Technology, Ministry of Agriculture and Rural Affairs, China Agricultural University, Beijing 100083, China*

Yuanjie Liu − *Key Laboratory of Agricultural Information Acquisition Technology, Ministry of Agriculture and Rural Affairs, China Agricultural University, Beijing 100083, China*

Yanbin Li − *Department of Biological and Agricultural Engineering, University of Arkansas, Fayetteville, Arkansas 72701, United States;* orcid.org/0000-0002-4142-7743

Complete contact information is available at: https://pubs.acs.org/10.1021/acssensors.1c00292

Notes

The authors declare no competing financial interest.

ACKNOWLEDGMENTS

This study was funded by the National Natural Science Foundation of China (Grant no. 32071899) and the Walmart Foundation (Project no. 61626817), and supported by the Walmart Food Safety Collaboration Center.

REFERENCES

(1) Shen, Y.; Xu, L.; Li, Y. Biosensors for rapid detection of Salmonella in food: A review. *Compr. Rev. Food Sci. Food Saf.* **2021**, *20*, 149−197.

(2) World Health Organization (WHO). Food safety, 2020, https://www.who.int/news-room/fact-sheets/detail/food-safety.

(3) Centers for Disease Control and Prevention (CDC), 2020. https://www.cdc.gov/salmonella/.

(4) Tsougeni, K.; Kaprou, G.; Loukas, C. M.; Papadakis, G.; Hamiot, A.; Eck, M.; Rabus, D.; Kokkoris, G.; Chatzandroulis, S.; Papadopoulos, V.; Dupuy, B.; Jobst, G.; Gizeli, E.; Tserepi, A.;

Gogolides, E. Lab-on-Chip platform and protocol for rapid foodborne pathogen detection comprising on-chip cell capture, lysis, DNA amplification and surface-acoustic-wave detection. *Sens. Actuators, B* **2020**, *320*, No. 128345.
(5) Xu, Z.; Long, L. L.; Chen, Y. Q.; Chen, M. L.; Cheng, Y. H. A nanozyme-linked immunosorbent assay based on metal-organic frameworks (MOFs) for sensitive detection of aflatoxin B1. *Food Chem.* **2021**, *338*, No. 128039.
(6) Zhou, Z.; Zhang, Y.; Guo, M.; Huang, K.; Xu, W. Ultrasensitive magnetic DNAzyme-copper nanoclusters fluorescent biosensor with triple amplification for the visual detection of *E. coli* O157:H7. *Biosens. Bioelectron.* **2020**, *167*, No. 112475.
(7) Zhu, W.; Chen, Y.; He, Y.; Fang, W.; Ying, Y.; Li, Y.; Fu, Y. Cooperation Mode of Outer Surface and Inner Space of Nanochannel: Separation-Detection System Based on Integrated Nanochannel Electrode for Rapid and Facile Detection of Salmonella. *Anal. Chem.* **2020**, *92*, 1818−1825.
(8) Poller, A. M.; Spieker, E.; Lieberzeit, P. A.; Preininger, C. Surface Imprints: Advantageous Application of Ready2use Materials for Bacterial Quartz-Crystal Microbalance Sensors. *ACS Appl. Mater. Interfaces* **2017**, *9*, 1129.
(9) Huang, Y.; Ren, J.; Qu, X. Nanozymes: Classification, Catalytic Mechanisms, Activity Regulation, and Applications. *Chem. Rev.* **2019**, *119*, 4357−4412.
(10) Liu, J.; Meng, L.; Fei, Z.; Dyson, P. J.; Zhang, L. On the origin of the synergy between the Pt nanoparticles and MnO2 nanosheets in Wonton-like 3D nanozyme oxidase mimics. *Biosens. Bioelectron.* **2018**, *121*, 159−165.
(11) Das, R.; Dhiman, A.; Kapil, A.; Bansal, V.; Sharma, T. K. Aptamer-mediated colorimetric and electrochemical detection of *Pseudomonas aeruginosa* utilizing peroxidase-mimic activity of gold NanoZyme. *Anal. Bioanal. Chem.* **2019**, *411*, 1229−1238.
(12) Zheng, L.; Cai, G.; Qi, W.; Wang, S.; Wang, M.; Lin, J. Optical Biosensor for Rapid Detection of *Salmonella typhimurium* Based on Porous Gold@Platinum Nanocatalysts and a 3D Fluidic Chip. *ACS Sens.* **2020**, *5*, 65−72.
(13) Chen, G.; Jin, M.; Ma, J.; Yan, M.; Cui, X.; Wang, Y.; Zhang, X.; Li, H.; Zheng, W.; Zhang, Y.; Abd El-Aty, A. M.; Hacimuftuoglu, A.; Wang, J. Competitive Bio-Barcode Immunoassay for Highly Sensitive Detection of Parathion Based on Bimetallic Nanozyme Catalysis. *J. Agric. Food Chem.* **2020**, *68*, 660−668.
(14) He, S. B.; Chen, F. Q.; Xiu, L. F.; Peng, H. P.; Deng, H. H.; Liu, A. L.; Chen, W.; Hong, G. L. Highly sensitive colorimetric sensor for detection of iodine ions using carboxylated chitosan-coated palladium nanozyme. *Anal. Bioanal. Chem.* **2020**, *412*, 499−506.
(15) Cheng, N.; Zhu, C.; Wang, Y.; Du, D.; Zhu, M.-J.; Luo, Y.; Xu, W.; Lin, Y. Nanozyme Enhanced Colorimetric Immunoassay for Naked-Eye Detection of *Salmonella enteritidis*. *J. Anal. Testing* **2019**, *3*, 99−106.
(16) Wu, J.; Lv, W.; Yang, Q.; Li, H.; Li, F. Label-free homogeneous electrochemical detection of MicroRNA based on target-induced anti-shielding against the catalytic activity of two-dimension nanozyme. *Biosens. Bioelectron.* **2021**, *171*, No. 112707.
(17) Ma, Y. D.; Li, K. H.; Chen, Y. H.; Lee, Y. M.; Chou, S. T.; Lai, Y. Y.; Huang, P. C.; Ma, H. P.; Lee, G. B. A sample-to-answer, portable platform for rapid detection of pathogens with a smartphone interface. *Lab Chip* **2019**, *19*, 3804−3814.
(18) Altintas, Z.; Akgun, M.; Kokturk, G.; Uludag, Y. A fully automated microfluidic-based electrochemical sensor for real-time bacteria detection. *Biosens. Bioelectron.* **2018**, *100*, 541−548.
(19) Wang, R.; Xu, Y.; Sors, T.; Irudayaraj, J.; Ren, W.; Wang, R. Impedimetric detection of bacteria by using a microfluidic chip and silver nanoparticle based signal enhancement. *Mikrochim. Acta* **2018**, *185*, No. 184.
(20) Cai, G.; Xue, L.; Zhang, H.; Lin, J. A Review on Micromixers. *Micromachines* **2017**, *8*, No. 274.
(21) Haghighinia, A.; Tabatabaei, S. M.; Movahedirad, S. A novel geometrically-hybrid microchannel for performance enhancement in mass transfer: Description of Lyapunov exponent and Poincaré map. *Int. J. Heat Mass Transfer* **2021**, *165*, No. 120700.
(22) Usefian, A.; Bayareh, M. Numerical and experimental investigation of an efficient convergent−divergent micromixer. *Meccanica* **2020**, *55*, 1025−1035.
(23) Mondal, B.; Mehta, S. K.; Patowari, P. K.; Pati, S. Numerical study of mixing in wavy micromixers: comparison between raccoon and serpentine mixer. *Chem. Eng. Process. - Process Intensification* **2019**, *136*, 44−61.
(24) Bayareh, M.; Ashani, M. N.; Usefian, A. Active and passive micromixers: A comprehensive review. *Chem. Eng. Process. - Process Intensification* **2020**, *147*, No. 107771.
(25) Wu, D.; Zhang, J.; Xu, F.; Wen, X.; Li, P.; Zhang, X.; Qiao, S.; Ge, S.; Xia, N.; Qian, S.; Qiu, X. A paper-based microfluidic Dot-ELISA system with smartphone for the detection of influenza A. *Microfluid. Nanofluid.* **2017**, *21*, No. 705.
(26) Ren, Y.; Wei, J.; He, Y.; Wang, Y.; Bai, M.; Zhang, C.; Luo, L.; Wang, J.; Wang, Y. Ultrasensitive label-free immunochromatographic strip sensor for Salmonella determination based on salt-induced aggregated gold nanoparticles. *Food Chem.* **2021**, *343*, No. 128518.
(27) Zeinhom, M. M. A.; Wang, Y.; Sheng, L.; Du, D.; Li, L.; Zhu, M.-J.; Lin, Y. Smart phone based immunosensor coupled with nanoflower signal amplification for rapid detection of Salmonella Enteritidis in milk, cheese and water. *Sens. Actuators, B* **2018**, *261*, 75−82.
(28) Guo, R.; Wang, S.; Huang, F.; Chen, Q.; Li, Y.; Liao, M.; Lin, J. Rapid detection of *Salmonella typhimurium* using magnetic nanoparticle immunoseparation, nanocluster signal amplification and smartphone image analysis. *Sens. Actuators, B* **2019**, *284*, 134−139.
(29) Zheng, L.; Cai, G.; Wang, S.; Liao, M.; Li, Y.; Lin, J. A microfluidic colorimetric biosensor for rapid detection of *Escherichia coli* O157:H7 using gold nanoparticle aggregation and smart phone imaging. *Biosens. Bioelectron.* **2019**, *124*−*125*, 143−149.
(30) Xue, L.; Huang, F.; Hao, L.; Cai, G.; Zheng, L.; Li, Y.; Lin, J. A sensitive immunoassay for simultaneous detection of foodborne pathogens using MnO2 nanoflowers-assisted loading and release of quantum dots. *Food Chem.* **2020**, *322*, No. 126719.
(31) Rath, D.; Kumar, S.; Panda, S. Enhancement of antigen−antibody kinetics on nanotextured silicon surfaces in mixed non-flow systems. *Mater. Sci. Eng., C* **2012**, *32*, 2223−2229.
(32) Chen, Q.; Wang, D.; Cai, G.; Xiong, Y.; Li, Y.; Wang, M.; Huo, H.; Lin, J. Fast and sensitive detection of foodborne pathogen using electrochemical impedance analysis, urease catalysis and microfluidics. *Biosens. Bioelectron.* **2016**, *86*, 770−776.
(33) Lu, J.; Kou, Y.; Jiang, X.; Wang, M.; Xue, Y.; Tian, B.; Tan, L. One-step preparation of poly(glyoxal-bis(2-hydroxyanil))-amino-functionalized graphene quantum dots-MnO2 composite on electrode surface for simultaneous determination of vitamin B2 and dopamine. *Colloids Surf., A* **2019**, *580*, No. 123652.
(34) Shan, S.; Liu, D.; Guo, Q.; Wu, S.; Chen, R.; Luo, K.; Hu, L.; Xiong, Y.; Lai, W. Sensitive detection of *Escherichia coli* O157:H7 based on cascade signal amplification in ELISA. *J. Dairy Sci.* **2016**, *99*, 7025−7032.
(35) Zhang, Z.; Wang, Q.; Han, L.; Du, S.; Yu, H.; Zhang, H. Rapid and sensitive detection of *Salmonella typhimurium* based on the photothermal effect of magnetic nanomaterials. *Sens. Actuators, B* **2018**, *268*, 188−194.
(36) Li, Q.; Xie, G.; Wang, Y.; Aguilar, Z. P.; Xu, H. Vancomycin-modified poly-l-lysine magnetic separation combined with multiplex polymerase chain reaction assay for efficient detection of *Bacillus cereus* in milk. *J. Dairy Sci.* **2021**, *104*, 1465−1473.
(37) Bahari, D.; Babamiri, B.; Salimi, A.; Salimizand, H. Ratiometric fluorescence resonance energy transfer aptasensor for highly sensitive and selective detection of *Acinetobacter baumannii* bacteria in urine sample using carbon dots as optical nanoprobes. *Talanta* **2021**, *221*, No. 121619.
(38) Srisa-Art, M.; Boehle, K. E.; Geiss, B. J.; Henry, C. S. Highly Sensitive Detection of *Salmonella typhimurium* Using a Colorimetric

https://doi.org/10.1021/acssensors.1c00292
ACS Sens. XXXX, XXX, XXX−XXX

Paper-Based Analytical Device Coupled with Immunomagnetic Separation. *Anal. Chem.* **2018**, *90*, 1035−1043.
(39) Zhou, J.; Tian, F.; Fu, R.; Yang, Y.; Jiao, B.; He, Y. Enzyme−Nanozyme Cascade Reaction-Mediated Etching of Gold Nanorods for the Detection of *Escherichia coli*. *ACS Appl. Nano Mater.* **2020**, *3*, 9016−9025.
(40) Asif, M.; Awan, F. R.; Khan, Q. M.; Ngamsom, B.; Pamme, N. Paper-based analytical devices for colorimetric detection of *S. aureus* and *E. coli* and their antibiotic resistant strains in milk. *Analyst* **2020**, *145*, 7320−7329.

https://doi.org/10.1021/acssensors.1c00292
ACS Sens. XXXX, XXX, XXX−XXX